Published in final edited form as:
Pigment Cell Melanoma Res. 2014 September ; 27(5): 831–834. doi:10.1111/pcmr.12278.

Support and challenges to the melanosomal casing model based on nanoscale distribution of metals within iris melanosomes detected by X-ray fluorescence analysis

Thomas Gorniak[1,2,3], **Tamás Haraszti**[2,4], **Heikki Suhonen**[5], **Yang Yang**[6], **Adam Hedberg-Buenz**[7,8], **Demelza Koehn**[8], **Ruth Heine**[6], **Michael Grunze**[1,2], **Axel Rosenhahn**[1,2,3,*], and **Michael G. Anderson**[7,8,*]

[1]Institute of Functional Interfaces (IFG), Karlsruhe Institute of Technology (KIT), Hermann-von-Helmholtz-Platz 1, 76344 Eggenstein-Leopoldshafen, Germany

[2]Applied Physical Chemistry, Ruprecht-Karls-University Heidelberg, Im Neuenheimer Feld 253, 69120 Heidelberg, Germany

[3]Analytical Chemistry - Biointerfaces, Ruhr-University Bochum, NC 4/27, 44801 Bochum, Germany

[4]Max-Planck-Institute for Intelligent Systems, Heisenbergstr. 3, 70569 Stuttgart, Germany

[5]ESRF, 6 rue Jules Horowitz, BP 220, F-38043 Grenoble Cedex, France

[6]Institute for Photon Science and Synchrotron Radiation (IPS), Karlsruhe Institute of Technology (KIT), Hermann-von-Helmholtz-Platz 1, 76344 Eggenstein-Leopoldshafen, Germany

[7]Department of Molecular Physiology and Biophysics, The University of Iowa, Iowa City, IA 52242, USA

[8]Center for the Prevention and Treatment of Visual Loss, Iowa City Veterans Affairs (VA) Health Care System, Iowa City, IA 52246, USA

Summary

Melanin within melanosomes exists as eumelanin or pheomelanin. Distributions of these melanins have been studied extensively within tissues, but less often within individual melanosomes. Here, we apply X-ray fluorescence analysis with synchrotron radiation to survey the nanoscale distribution of metals within purified melanosomes of mice. The study allows a discovery-based characterization of melanosomal metals, and, because Cu is specifically associated with eumelanin, a hypothesis-based test of the “casing model” predicting that melanosomes contain a pheomelanin core surrounded by a eumelanin shell. Analysis of Cu, Ca, and Zn shows variable concentrations and distributions, with Ca/Zn highly correlated, and at least three discrete patterns for the distribution of Cu vs. Ca/Zn in different melanosomes – including one with a Cu-rich shell surrounding a Ca/Zn-rich core. Thus, the results support predictions of the casing model, but also

*CORRESPONDANCE Michael G. Anderson and Axel Rosenhahn, MGA: michael-g-anderson@uiowa.edu, phone +1 (319) 335 7839, FAX +1 (319) 335 7330, AR: axel.rosenhahn@rub.de, phone +49 234 3224200, FAX: +49 234 3214420.
*These authors contributed equally to this work.

suggest that in at least some tissues and genetic contexts, other arrangements of melanin may co-exist.

Keywords

Melanosome; metal; eumelanin; pheomelanin; X-ray fluorescence analysis; synchrotron-based imaging

Mammalian melanin exists in two chemically distinct forms, black to brown eumelanin and yellow to reddish-brown pheomelanin (Simon and Peles, 2010). In addition to contributing to the color of tissues, the differing physiochemical properties of eumelanin and pheomelanin – especially their opposing anti-oxidant and pro-oxidant natures – likely influence several diseases (Simon et al., 2009). While their distribution has been studied extensively within whole tissues (Ito and Wakamatsu, 2003) the spatial organization of eumelanin and pheomelanin at the level of melanosomes has been more difficult to investigate. Based on biochemical findings, Agrup et al. (1982) proposed a “casing model” that predicts individual melanosomes to contain a pheomelanin core surrounded by a eumelanin shell. Since then, additional support for the casing model has come from two primary sources: predictions based on the intrinsic chemical reactivity of ortho-quinones (Ito and Wakamatsu, 2008) and direct measurements of surface ionization thresholds of melanin (Bush et al., 2006; Peles et al., 2009). Thus, while the model is widely accepted, it has also been somewhat recalcitrant to other forms of direct experimentation that might challenge or confirm it.

Recent advances in nanoscale imaging of trace elements using synchrotron-based techniques offer a new opportunity for studying melanin distribution within melanosomes. Synchrotron radiation has several features ideal for nanoscale applications and can be tuned to study specific elements, including metals. Melanin is known to contain a variety of metal ions (Hong and Simon, 2007), including metals with unique properties specific to sub-types of melanin. For example, copper (Cu) promotes eumelanogenesis (Ito et al., 2013) and its high affinity for eumelanin allows it to be used as a surrogate marker for eumelanin distribution (Wogelius et al., 2011). X-ray fluorescence (XRF) analysis with synchrotron radiation allows visualization of metals at the nanoscale by irradiating a sample region with focused X-rays and detecting emitted fluorescence photons characteristic for specific elements. Thus, XRF studies of Cu distribution in melanosomes offer a new opportunity for testing the casing model, and at the same time allow the distribution of other metals within melanosomes to be discovered at sub 100-nm resolution.

To apply XRF analysis to melanosome samples, iridial sucrose gradient-purified melanosomes from inbred strains of mice were prepared (vitrified and subsequently freeze-dried) and studied using the ID22NI end-station of the European Synchrotron Radiation Facility (ESRF) in Grenoble, France (Martinez-Criado et al., 2012). For additional details on methods, see Supporting information S1.

Results of this experiment showed robust signatures for copper (Cu), calcium (Ca) and zinc (Zn). There was no contrast in substrate versus melanosome for iron, suggesting that either

its amount was below the limit of detection or that the metal has a low affinity for melanosomes and was diluted away during the melanosome preparation. Color-coded XRF maps show variable amounts of metals per melanosome, sometimes organized into non-random distribution patterns (Figure 1A–F). The most striking pattern observed is one in which the Cu-signal is highest at the melanosomal periphery, whereas Ca- and Zn-signals are highest in their centers. To further assess the nature of these complementary distributions, organelles were segmented, i.e. the signal was separated from the background (details in Supporting information S1). Cu, Ca and Zn intensities were normalized to their maximum values, and finally, the data was merged into RGB images (Figure 1G, H). From the color distribution it becomes apparent that within some melanosomes Ca and Zn are concentrated within their core regions. Simultaneously, Cu is more likely to be found close to their surface. Because Cu is a marker of eumelanin (Wogelius et al., 2011), visualization of melanosomes with this pattern directly supports predictions of the casing model.

However, additional patterns of metal distribution were also observed. These differences are particularly evident from scatter plots expressing the mass ratios of different metals per pixel within images of single melanosomes (Figure 2). In all melanosomes analyzed, the occurrence of Ca and Zn were highly correlated (Supporting information S1, Figure S1). In contrast, comparisons of Cu versus Ca/Zn revealed complex correlations identifying at least three distinct classes of melanosomes, visible as three separate clouds of data points (colored red, green and orange/blue) in Figure 2. As discussed above, one class was characterized by a Cu-rich periphery and Ca/Zn-rich center (see orange and blue data points in Figure 2A). The other main classes of melanosomes, which were observed in the DBA/2J dataset, were characterized by distinct types of homogeneous metal distributions described by different slopes of the fitted functions (see green and red data points in Figure 2B).

To our knowledge, this study represents the first time that XRF imaging has been utilized to study the metal composition of melanosomes at a sub-organelle level. Several conclusions can be drawn. First, as others have shown, melanosomes contain several metals of biological relevance (Biesemeier et al., 2011; Hong and Simon, 2007). Second, the peripheral enrichment of Cu supports the casing model – at least for some melanosomes. It is interesting to note that Zn promotes several aspects of pheomelanogenesis (Napolitano et al., 2008; 2001; Panzella et al., 2010), thus, it may constitute a reciprocal marker of pheomelanin. Finally, in at least the iris melanosomes of DBA/2J mice, three distinct classes of melanosomes can be inferred to exist based on their patterns of metal distribution, including some with homogenous patterns of Cu and Ca/Zn. One interpretation of this observation is that in at least some melanosomes, the spatial domains of eumelanin and pheomelanin overlap such that their signals are not distinct – an apparent challenge to the casing model. Alternatively, it is possible that some melanosomes were physically damaged during purification, destroying our ability to discern the native pattern. Our experiment described here does not distinguish these possibilities, only that the nanoscale distribution of metals seem to identify multiple distinct classes of melanosomes.

Among potential caveats influencing these experiments, issues of sample size, genetic background, and tissue heterogeneity warrant particular mention. Beam time at synchrotron facilities is in high demand, and experiments often require years of advance planning. Our

current experiments were conducted within a single visit through a collaborative arrangement. While the results obtained to date should promote the likelihood of groups acquiring additional beam time to build on this work, the current sample size is admittedly – and unavoidably – limited. In future work, it would also be particularly interesting to dissect the influence that genetic background plays in each of the observed features, as well as relating how the observed variations may correlate to the differing developmental origins of melanosomes from the neural crest-derived melanocytes of the iris stroma versus neuroepithelial-derived cells of the iris pigment epithelium. The *Tyrp1*^{b} mutation found in DBA/2J mice, which is known to influence the morphology and levels of eumelanin, but not pheomelanin, in melanocyte cultures (Hirobe et al., 2014), will be particularly interesting as it remains unknown if mutations such as this that influence bulk eumelanin to pheomelanin ratios might also scale to influence features of individual melanosomes.

In conclusion, we have shown that nanoscale XRF can distinguish multiple patterns of metal distribution within iris melanosomes of mice. The observation of some melanosomes with a Cu-rich periphery supports the casing model, whereas the observation of homogenous metal distributions in other melanosomes challenges this model and suggests that in at least some tissues and genetic contexts, other arrangements of melanin may co-exist.

Supplementary Material

Refer to Web version on PubMed Central for supplementary material.

Acknowledgments

We gratefully acknowledge funding by the Virtual Institute VH-VI-403 and National Eye Institute Grant EY017673. We also acknowledge the European Synchrotron Radiation Facility for provision of synchrotron radiation facilities.

References

Agrup G, Hansson C, Rorsman H, Rosengren E. The effect of cysteine on oxidation of tyrosine, dopa, and cysteinyldopas. Arch Dermatol Res. 1982; 272:103–115. [PubMed: 6819815]

Biesemeier A, Schraermeyer U, Eibl O. Quantitative chemical analysis of ocular melanosomes in stained and non-stained tissues. Micron. 2011; 42:461–470. [PubMed: 21330141]

Bush WD, Garguilo J, Zucca FA, Albertini A, Zecca L, Edwards GS, Nemanich RJ, Simon JD. The surface oxidation potential of human neuromelanin reveals a spherical architecture with a pheomelanin core and a eumelanin surface. PNAS. 2006; 103:14785–14789. [PubMed: 17001010]

Hirobe T, Ito S, Wakamatsu K, Kawa Y, Abe H. The Mouse Brown (b/Tyrp1b) Allele Does Not Affect Pheomelanin Synthesis in Mice. Zoological Science. 2014; 31:53–63. [PubMed: 24521313]

Hong L, Simon JD. Current understanding of the binding sites, capacity, affinity, and biological significance of metals in melanin. J Phys Chem B. 2007; 111:7938–7947. [PubMed: 17580858]

Ito S, Wakamatsu K. Quantitative Analysis of Eumelanin and Pheomelanin in Humans, Mice, and Other Animals: a Comparative Review. Pigment Cell Res. 2003; 16:523–531. [PubMed: 12950732]

Ito S, Wakamatsu K. Chemistry of Mixed Melanogenesis—Pivotal Roles of Dopaquinone. Photochem Photobiol. 2008; 84:582–592. [PubMed: 18435614]

Ito S, Suzuki N, Takebayashi S, Commo S, Wakamatsu K. Neutral pH and copper ions promote eumelanogenesis after the dopachrome stage. Pigment Cell Melanoma Res. 2013; 26:817–825. [PubMed: 23844795]

Martinez-Criado G, Tucoulou R, Cloetens P, et al. Status of the hard X-ray microprobe beamline ID22 of the European Synchrotron Radiation Facility. J Synchrotron Rad. 2012; 19:10–18.

Napolitano A, De Lucia M, Panzella L, d'ischia M. The "benzothiazine" chromophore of pheomelanins: a reassessment. Photochem Photobiol. 2008; 84:593–599. [PubMed: 18435615]

Napolitano A, Di Donato P, Prota G. Zinc-catalyzed oxidation of 5-S-cysteinyldopa to 2,2′-bi(2H-1,4-benzothiazine): tracking the biosynthetic pathway of trichochromes, the characteristic pigments of red hair. J Org Chem. 2001; 66:6958–6966. [PubMed: 11597214]

Panzella L, Szewczyk G, d'ischia M, Napolitano A, Sarna T. Zinc-induced Structural Effects Enhance Oxygen Consumption and Superoxide Generation in Synthetic Pheomelanins on UVA/Visible Light Irradiation†. Photochem Photobiol. 2010; 86:757–764. [PubMed: 20408987]

Peles DN, Hong L, Hu DN, Ito S, Nemanich RJ, Simon JD. Human Iridal Stroma Melanosomes of Varying Pheomelanin Contents Possess a Common Eumelanic Outer Surface. J Phys Chem B. 2009; 113:11346–11351. [PubMed: 19618947]

Simon JD, Peles DN. The Red and the Black. Acc Chem Res. 2010; 43:1452–1460. [PubMed: 20734991]

Simon JD, Peles D, Wakamatsu K, Ito S. Current challenges in understanding melanogenesis: bridging chemistry, biological control, morphology, and function. Pigment Cell Melanoma Res. 2009; 22:563–579. [PubMed: 19627559]

Wogelius RA, Manning PL, Barden HE, et al. Trace Metals as Biomarkers for Eumelanin Pigment in the Fossil Record. Science. 2011; 333:1622–1626. [PubMed: 21719643]

Significance

Here, we utilize synchrotron-based imaging to study nanoscale metal distributions within purified melanosomes of mice – the first time metals have been observed in melanosomes at this resolution. The results show discrete patterns of metal distribution that vary between melanosomes and challenge current models concerning the organization of eumelanin and pheomelanin within these organelles.

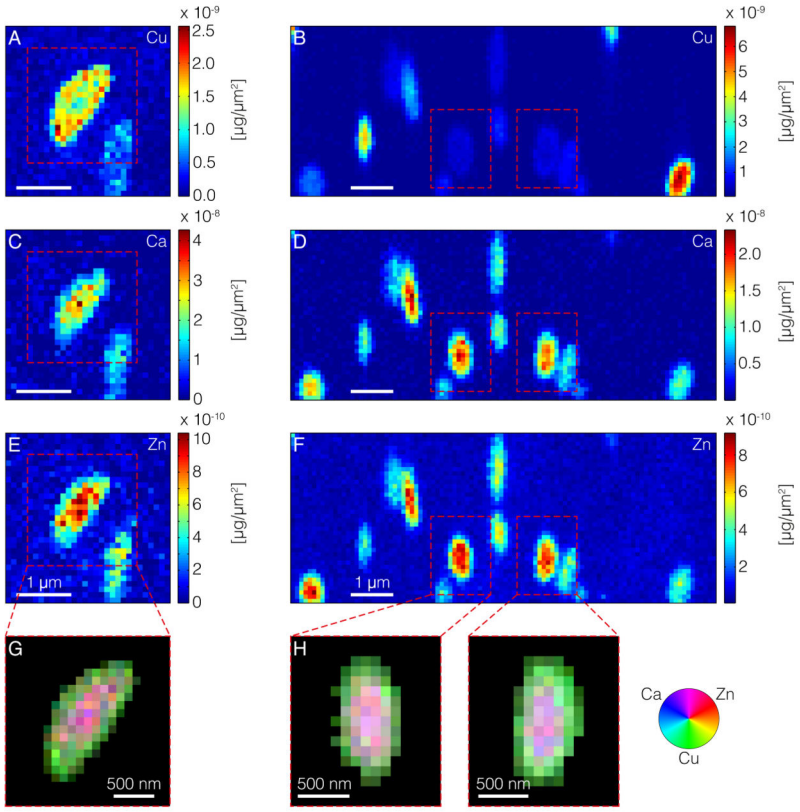

Figure 1.

Spatial distributions of metals in purified iridial melanosomes from C57BL/6J (*left*) and DBA/2J (*right*) mice, showing Cu (A, B), Ca (C, D), and Zn (E, F). As indicated by the color bar next to the maps, blue represents low concentrations and red high concentrations. (G, H) Segmented correlative maps of metal distributions. The colors shown in the color wheel are RGB composites obtained by adding the red, blue and green color channels. The intensities in each of the channel are proportional to the local concentrations of Ca (*blue*), Zn (*red*), and Cu (*green*).

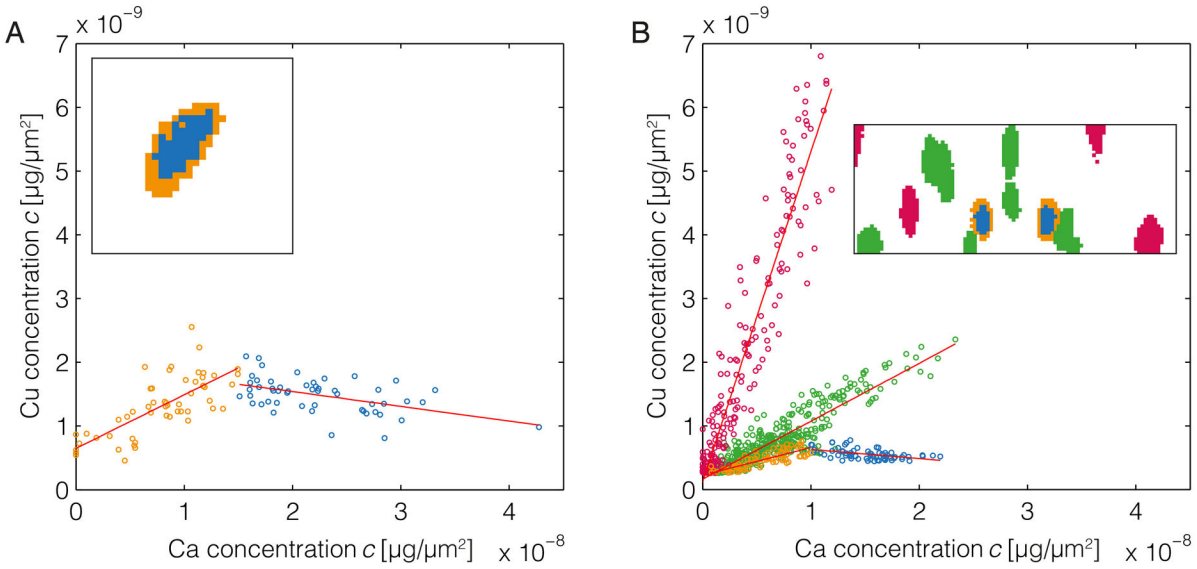

Figure 2.

Scatter plots of Cu and Ca concentrations in purified iridial melanosomes from C57BL/6J (left) and DBA/2J (right) mice. Data points are color-coded to indicate their origin from real space pixels as shown in the insets. (A) The scatter plot for the C57BL/6J dataset shows a single (class of) melanosome characterized by a peripheral region of positive correlation (*orange*) and a central region of negative correlation (*blue*). The fitted functions yield a slope of $m_{o,A} = 0.085$ for orange-colored data points and $m_{b,A} = -0.025$ for the blue-colored points. There is also a single organelle not shown here, which by visual inspection appears to show a trend for peripheral Cu and central Ca/Zn enrichment (evident in the lower right portion of Figures 1A, C, and E) but is omitted from this analysis because it contains too few pixels for a meaningful correlation examination. (B) The scatter plot of Cu and Ca based on the DBA/2J dataset reveals three classes of melanosomes: organelles with a comparatively high Cu/Ca mass ratio (*red*, $m_{r,B} = 0.519$), organelles with a comparatively low metal mass ratio (*green*, $m_{g,B} = 0.091$) – both classes with an overall positive correlation – and organelles with a core that features a negative Cu vs. Ca correlation (*orange*, $m_{o,B} = 0.044$; and *blue*, $m_{b,B} = -0.015$). Results are shown for Cu/Ca, but because Ca and Zn are highly correlated (see Figure S1), the results are also valid for the pair Cu/Zn.